Geophysical Research Letters

RESEARCH LETTER
10.1029/2018GL080644

Tsunami Wavefield Reconstruction and Forecasting Using the Ensemble Kalman Filter

Yuyun Yang[1], Eric M. Dunham[1,2], Guillaume Barnier[2], and Martin Almquist[2]

[1]Institute for Computational and Mathematical Engineering, Stanford University, Stanford, CA, USA, [2]Department of Geophysics, Stanford University, Stanford, CA, USA

Key Points:
- We propose an alternative tsunami wavefield assimilation method, the ensemble Kalman filter
- The methods are tested on scenario tsunami in Cascadia from fully coupled dynamic earthquake and tsunami simulation
- Ensemble Kalman filter achieved more accurate and stable forecasts compared to optimal interpolation

Supporting Information:
- Supporting Information S1
- Figure S1
- Figure S2
- Figure S3
- Figure S4

Correspondence to:
Y. Yang,
yyang85@stanford.edu

Citation:
Yang, Y., Dunham, E. M., Barnier, G., & Almquist, M. (2019). Tsunami wavefield reconstruction and forecasting using the ensemble Kalman filter. *Geophysical Research Letters*, *46*, 853–860. https://doi.org/10.1029/2018GL080644

Received 26 SEP 2018
Accepted 7 JAN 2019
Accepted article online 15 JAN 2019
Published online 29 JAN 2019

Abstract Offshore sensor networks like DONET and S-NET, providing real-time estimates of wave height through measurements of pressure changes along the seafloor, are revolutionizing local tsunami early warning. Data assimilation techniques, in particular, optimal interpolation (OI), provide real-time wavefield reconstructions and forecasts. Here we explore an alternative assimilation method, the ensemble Kalman filter (EnKF), and compare it to OI. The methods are tested on a scenario tsunami in the Cascadia subduction zone, obtained from a 2-D coupled dynamic earthquake and tsunami simulation. Data assimilation uses a 1-D linear long-wave model. We find that EnKF achieves more accurate and stable forecasts than OI, both at the coast and across the entire domain, especially for large station spacing. Although EnKF is more computationally expensive than OI, with development in high-performance computing, it is a promising candidate for real-time local tsunami early warning.

Plain Language Summary Recent years have seen more research on tsunami early warning using data from seafloor pressure sensors. Forecasts of the tsunami wave height can be computed by incorporating the pressure observations into the physical model of wave propagation. The current approach uses a simple, constant linear interpolator to blend the data with the model forecast. To improve the accuracy and stability of the forecast, we propose a more mathematically sophisticated approach that dynamically updates this interpolator, as the physical model evolves and as more data become available. This will incorporate more information into the forecast and optimize it. Using a scenario tsunami from our earthquake-tsunami coupled simulation in the Cascadia subduction zone, we run our proposed data assimilation approach. The predicted wave heights across the ocean and at the coast are more accurate and consistent over time. More reliable forecasts can therefore be issued to coastal residents earlier in the event of a destructive tsunami. Although our method takes longer to run, with greater computing power and more efficient implementation, it is a promising candidate for real-time tsunami early warning.

1. Introduction

The devastating 2004 Sumatra and 2011 Tohoku earthquakes, generating massive tsunamis and costing tens of thousands of lives, sparked research on novel techniques for local tsunami forecasts. The traditional approach to tsunami early warning is based on seismic source inversion using data from onshore seismometer networks. The inverted earthquake hypocenter and magnitude are input into a database of precomputed tsunami scenarios to predict tsunami arrival time and maximum wave height (Hoshiba & Ozaki, 2014). There have been suggestions to update these forecasts using finite-fault slip inversions from high-rate Global Navigation Satellite System data (Blewitt et al., 2009; Melgar et al., 2016; Melgar & Bock, 2013; Tsushima et al., 2014; Xu & Song, 2013).

However, tsunami forecast methods based on earthquake source inversions have some disadvantages. First, uncertainties in source parameter estimates propagate into the tsunami forecasts (Titov et al., 2005). Second, an elastic Earth response is assumed in going from earthquake to tsunami, which might be violated due to yielding of sediments (Ma, 2012). Finally, seismic inversions can overlook tsunamis caused by landslides or tsunami earthquakes (Maeda et al., 2015).

To address these issues, one can directly measure tsunamis using ocean bottom pressure gauges (OBPGs) that stream real-time data. Japan has such networks along the Japan Trench (S-NET; Yamamoto et al., 2016) and the Nankai Trough subduction zone (DONET; Kawaguchi et al., 2008). The Cascadia subduction

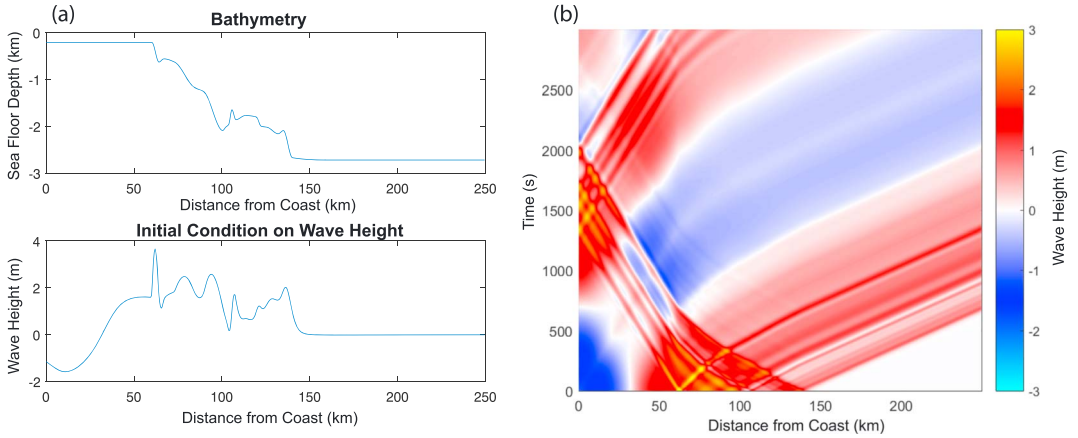

Figure 1. Scenario tsunami simulation used in this study. (a) Bathymetry, (b) initial wave height, and (c) space-time plot of wave height. The rupture extends from coast to approximately 140 km offshore. Large-amplitude waves arrive at the coast between ~1,000 and 2,000 s, with several of the largest arrivals emanating from short-wavelength bathymetric features.

zone has instruments from Northeast Pacific Time-Series Undersea Networked Experiments (NEPTUNE)-Canada (Thomson et al., 2011) and Ocean Observatories Initiative cabled arrays (Toomey et al., 2014). Offshore data can be used to invert for tsunami initial conditions (Tsushima et al., 2011) or to reconstruct the tsunami wavefield using sequential data assimilation methods (Gusman et al., 2016; Maeda et al., 2015). Previous data assimilation studies have used optimal interpolation (OI), a simplified version of the Kalman filter (KF) that keeps both the Kalman gain matrix and error covariance matrix fixed throughout assimilation. This provides computational efficiency, particularly when exploiting linearity to use Green's functions to make forecasts at select locations (Wang et al., 2017). However, as we demonstrate in this study, improved stability and accuracy can be achieved by updating the gain and error covariance matrices.

In this study, we introduce the ensemble Kalman filter (EnKF) for tsunami data assimilation and compare it to OI using tsunami signals from synthetic OBPG networks. We find that EnKF results are more accurate and stable, at the cost of additional computational expense.

2. Tsunami Simulation

We apply the OI and EnKF methods to a scenario tsunami for the Cascadia subduction zone (Figure 1), governed by the linear long-wave equations in 1-D:

$$\partial\eta/\partial t = -\partial q/\partial x, \quad \partial q/\partial t = -gH\partial\eta/\partial x, \tag{1}$$

where x is horizontal distance offshore from the coast, $\eta(x,t)$ is wave height, $q(x,t)$ is horizontal flux, g is gravitational acceleration, and $H(x)$ is ocean depth. These equations are solved using fourth-order summation-by-parts finite difference operators on a staggered grid (O'Reilly et al., 2017), a fourth-order Runge-Kutta method for time stepping, with $q(0,t) = 0$ at the coast and a nonreflecting boundary condition far offshore. The grid spacing is 0.5 km, and the time step is 1.5 s. Tsunami initial conditions are taken from a fully coupled 2-D simulation of the earthquake and tsunami in Lotto et al. (2018) using the methodology of Kozdon et al. (2013) and Lotto and Dunham (2015). This simulation captures seismic, ocean acoustic, and tsunami waves, with heterogeneous material structure and bathymetry.

3. EnKF

Data assimilation methods improve the forecast from the physical model—in this study, equation (1)—by incorporating observations at certain time intervals. One of these methods is KF, which produces estimates of the wave height given the observations, the physical model, and their error covariance matrices. At each assimilation time step, we first use the physical model to compute a prior estimate then obtain the posterior estimate via linear interpolation between the prior and the data. This interpolation operator is the gain matrix, which is updated after each step to minimize the posterior error covariance.

We now present the KF method. Define the state variable (wave height η and flux q at discrete grid points) at time step k to be x_k. This corresponds to the true wavefield, which is unknown but can be estimated. At time $k-1$, the best estimate of x_{k-1} is $\hat{x}_{k-1}$. Let F_k represent how the physical process evolves in one time step from $k-1$ to k (i.e., the linear matrix operator for the discretized, equation (1)). Let P_{k-1} be the covariance matrix of $\hat{x}_{k-1}$. The predicted mean of x_k and its covariance matrix are calculated via equation (2), with the superscript $^-$ representing the prior:

$$\hat{x}_k^- = F_k \hat{x}_{k-1}, \quad P_k^- = F_k P_{k-1} F_k^T. \tag{2}$$

To incorporate data, let H be the observation matrix (such that Hx_k provides the wave height at sensor locations). Then the distribution (assumed to be normal) of the predicted observations from the prior has mean $H\hat{x}_k^-$ and covariance $HP_k^-H^T$. Let the actual observations be z_k (assumed to be normal) and the covariance of observational error be R_k (R is kept constant in this work). To optimally blend the prior estimate and the actual observation, we calculate the posterior distribution as follows:

$$\hat{x}_k = \hat{x}_k^- + K_k(z_k - H\hat{x}_k^-), \quad P_k = (I - K_k H)P_k^-, \tag{3}$$

where the Kalman gain is

$$K_k = P_k^- H^T (HP_k^- H^T + R_k)^{-1}. \tag{4}$$

Equations (2)–(4) represent the prediction and update steps in KF.

EnKF is a stochastic approximation of KF with reduced computational expense and memory usage (Madsen & Canizares, 1999). EnKF starts with an initial ensemble (with N members) drawn from the distribution of wave height η and flux q at $t = 0$. We assume the mean of the distribution to be 0 for both η and q. We propagate this ensemble forward in time the same way as in KF, obtaining a distribution of wave heights at the coast from which a statistical forecast can be made.

There are three main differences between EnKF and KF:

1. There is an ensemble of predicted means $\hat{X}_k^- = [\hat{x}_k^{-(1)}, \ldots, \hat{x}_k^{-(N)}]$ instead of a single estimate at time k.
2. P_k^- is directly calculated as $\mathrm{Cov}(\hat{X}_k^-)$ instead of applying equation (2). There is also no need to calculate P_k. Thus, instead of storing a full covariance matrix, we represent the same error statistics using an ensemble of model states: an approximation and a form of dimensionality reduction. As the size of the ensemble N increases, error in the Monte Carlo sampling decreases as $N^{-1/2}$ (Evensen, 2003).
3. We draw N perturbations $v_k^{(i)}$ to add to the observations, which are treated as random variables. For ensemble member i ($i = 1, \ldots, N$),

$$\hat{x}_k^{(i)} = \hat{x}_k^{-(i)} + K_k(z_k + v_k^{(i)} - H_k\hat{x}_k^{-(i)}). \tag{5}$$

As the ensemble size $N \to \infty$, EnKF converges to KF for linear Gaussian models (Katzfuss et al., 2016). See the supporting information for more details on why KF is an optimization method (Aravkin et al., 2014).

The OI method is a greater simplification of KF and less optimal than EnKF, using only the first two members of equations (2) and (3), keeping the error covariance matrix P and the Kalman gain matrix K constant throughout the assimilation.

4. Data Assimilation Using EnKF

To examine the accuracy and stability of EnKF compared to OI, there are two key parameters that we varied:

1. Station spacing (Δx_{stn}). Tsunami wavelengths shorter than $2\Delta x_{\mathrm{stn}}$ will be spatial aliased, resulting in poor waveform agreement (Maeda et al., 2015). We experimented with $\Delta x_{\mathrm{stn}} = 15$, 30, and 50 km, since the DONET spacing is 15–20 km (Tonegawa et al., 2017), and the S-NET spacing is 30–50 km (Maeda et al., 2015).
2. Assimilation time interval ($\Delta t_{\mathrm{assim}}$). In reality, we may need to process the pressure signals (e.g., to remove seismic waves or correct for nonhydrostatic ocean response) before they can be assimilated. We may also want to assimilate less often due to computational cost. We experimented with $\Delta t_{\mathrm{assim}} = 3$ and 15 s. This means that although our time step is 1.5 s, for $\Delta t_{\mathrm{assim}} = 3$ s, we propagate the wave height and flux for two time steps before we assimilate any data.

We set up an initial Gaussian error covariance matrix P_0 with characteristic length of 20 km. P_0 has a block diagonal structure, one block representing the covariance matrix for the wave height η, and the other block the covariance matrix for the flux q. We choose the initial standard deviation for η to be 0.15 m. The higher this value is compared to the error standard deviation of the observations, the less we trust the physics model and the more we trust the data. For q, we set its initial standard deviation to 0, which we found to result in the most accurate forecasts.

Observations come from normal random perturbations of the true solution with standard deviation 0.05 m. The error covariance matrix of the observations, R, is diagonal with standard deviation 0.05 m, so that errors are independent. The ensemble size is $N = 100$, and we forecast every 30 s. Making a forecast means advancing the ensemble using the physics model only with no further data assimilation, and this can be done at any time. We report only the ensemble mean of the forecast here.

In the following section, we focus on the effects of station spacing for $\Delta x_{\text{stn}} = 30$ and 50 km, fixing $\Delta t_{\text{assim}} = 3$ s. Results for other choices of Δx_{stn} and Δt_{assim} are provided in the supporting information.

5. Results

5.1. Base Case: $\Delta t_{\text{assim}} = 3$ s, $\Delta x_{\text{stn}} = 30$ km

We first examine the case with assimilation time interval $\Delta t_{\text{assim}} = 3$ s and station spacing $\Delta x_{\text{stn}} = 30$ km. Figure 2 shows the EnKF and OI forecasts at 150 and 600 s. The dashed lines in Figures 2a–2d represent the 150- and 600-s separators, respectively: Above them, we show the entire forecast waveform from 150 or 600 s onward; below them, we show the results from the closest previous forecast at 30-s intervals. As the forecast for the same location improves over time due to more data being assimilated, we can notice horizontal strips in these figures, each separated by the forecast time interval of 30 s. For example, the 0- to 30-s forecast is based on the initial condition (which is set to be 0, so the forecast is also 0), and the 30- to 60-s forecast is based on the assimilated data up to 30 s, etc.

We make three observations based on Figure 2. First, the EnKF forecasts improve significantly from 150 to 600 s, showing the importance of allowing time for more data to be assimilated. Its improvement is also greater than OI's. Second, EnKF achieves a waveform closer to the true solution than OI and can resolve more details for shorter wavelengths (e.g., the large-amplitude wave arriving around 2,000 s). Finally, the previous forecasts of EnKF are more consistent with one another compared to OI.

Figure 2e shows five full forecasts of the wave height at the coast, with the forecasts performed at successively later times as marked, before the maximum wave height hits the coast. Note that the shorter-wavelength waves arriving around 1,400–1,600 s are smoothed out in the forecasts for both EnKF and OI compared, due to shorter wavelengths than the station spacing. Nevertheless, EnKF captures the peaks around 1,600 and 2,000 s very well, whereas OI misses these details. The EnKF forecasts agree nicely with the true solution except for the first two peaks, where the wave height suffers from a slight underestimation. The fit gets better for later forecasts especially for EnKF, as more data are assimilated. This is natural as the continual update of the Kalman gain matrix in EnKF allows the method to capture the physical evolution of the system with increasing accuracy.

Figure 2f shows forecasts of the maximum wave height and its arrival time, compared to the true solution. EnKF achieves a forecast that is close to the true maximum wave height with less fluctuation than OI. The consistent underestimation here is dependent the initial error covariance matrix and wave height distribution that we choose for the ensemble. The arrival time forecasts are similar and are overestimated due to the effect we see in Figure 2e: As the shorter-wavelength components are smoothed out, the first peak of the coastal wave is not reconstructed. Rather, the higher waves concentrate near 1,500–1,600 s.

Supporting information includes more comparison plots for this scenario and the evolution of the error standard deviation of the covariance matrix in EnKF.

5.2. Effects of Varying Station Spacing

Due to spatial aliasing, as the wavelength decreases relative to station spacing, the quality of data assimilation decreases (Maeda et al., 2015). We purposely chose a scenario tsunami featuring multiple, closely spaced peaks from short-wavelength waves (Figure 1b). These features get smoothed out in both EnKF and OI, with the former preserving higher resolution. Here, we examine how these two methods compare when the station spacing is wider.

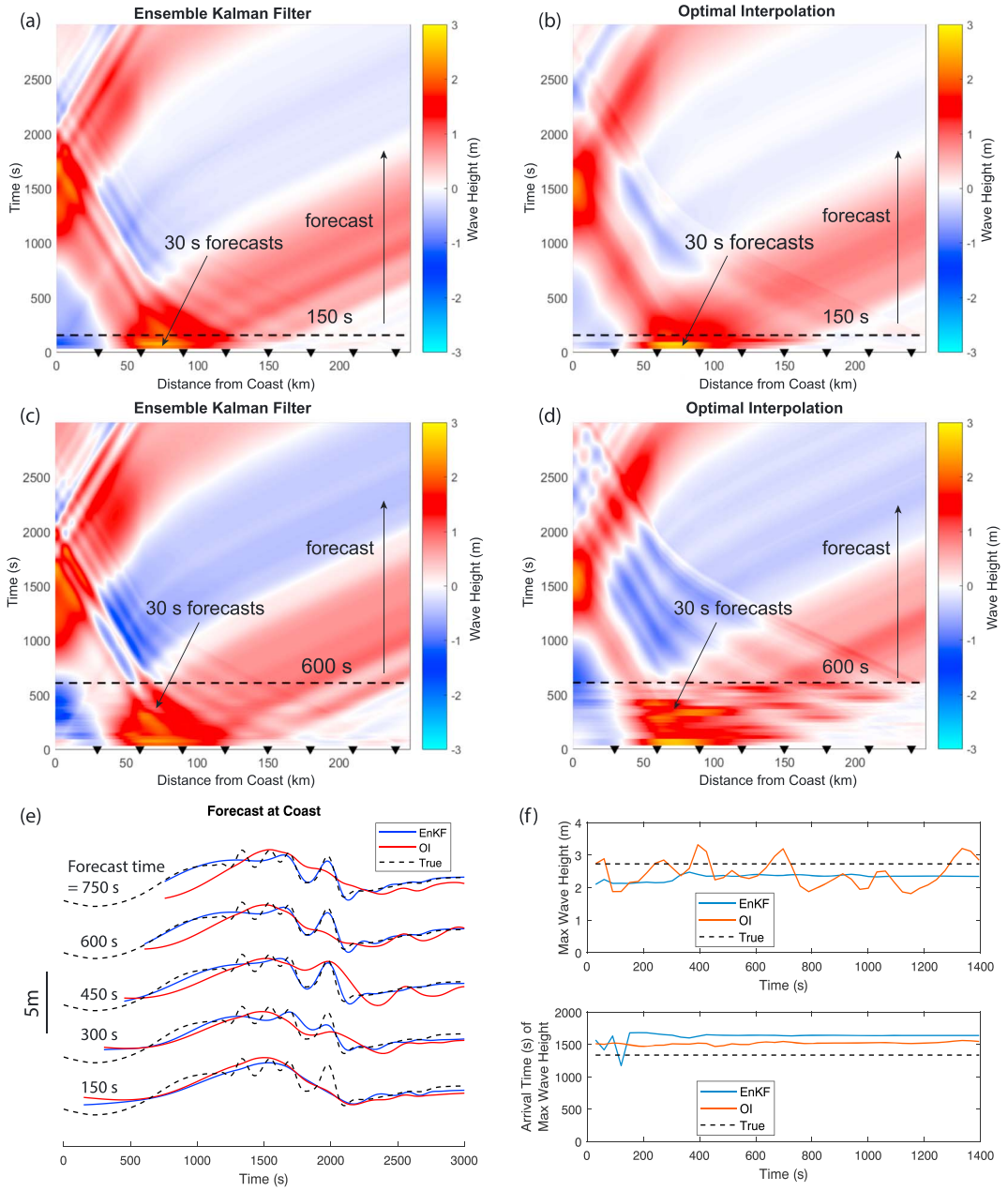

Figure 2. $\Delta x_{\text{stn}} = 30$ km, $\Delta t_{\text{assim}} = 3$ s. (a)–(d) Wave height forecasts, updated every 30 s below the horizontal dashed line for EnKF (a and c) and OI (b and d), with stations marked by inverted triangles. The forecast after 600 s (c and d) improves relative to the forecast after 150 s (a and b). (e) Coastal wave height forecasts starting at different times, showing improved predictions with more assimilated data. In general, EnKF is more accurate and better able to resolve finer details than OI. (f) Forecasts of maximum wave height and arrival time at the coast. EnKF = ensemble Kalman filter; OI = optimal interpolation.

Figure 3 shows the results when $\Delta x_{\text{stn}} = 50$ km, $\Delta t_{\text{assim}} = 3$ s. In Figures 3a–3d, EnKF's outperformance is even more apparent in how its waveform is much closer to the true waveform than OI and how it preserves many details of the shorter wavelengths with such sparse station coverage. The clear advantage of updating the Kalman gain matrix and error covariance matrix can be seen from the contrast between the forecast at 150 and at 600 s: Although initially, EnKF and OI performed equally badly due to fewer stations, through the assimilation and update, EnKF manages to reconstruct the waveform well after some time, whereas OI does not substantially improve.

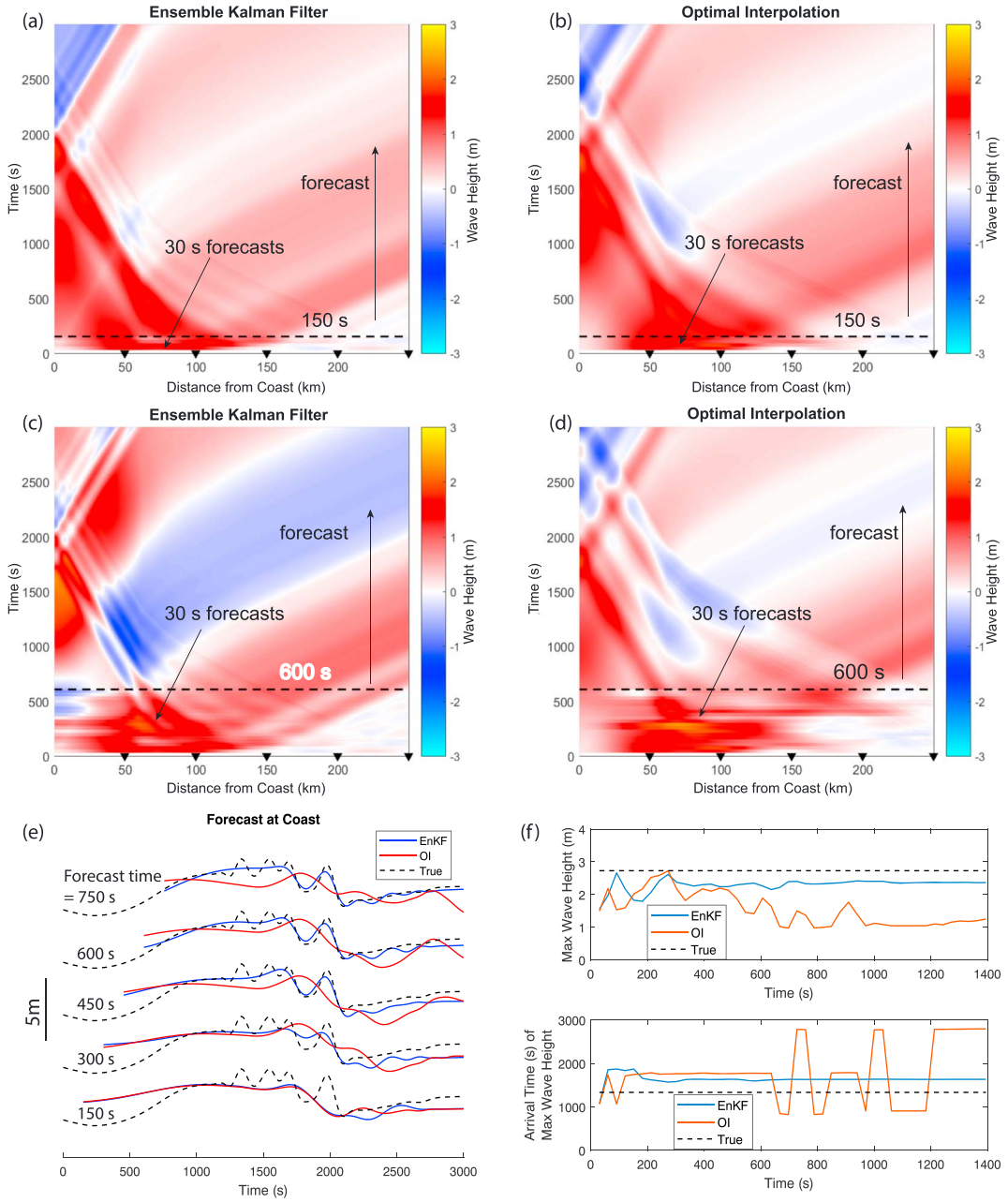

Figure 3. Same as Figure 2 but for larger station spacing: $\Delta x_{\text{stn}} = 50$ km, $\Delta t_{\text{assim}} = 3$ s. Neither EnKF nor OI can make accurate forecasts for early times, but the EnKF improves with additional data assimilation and is able to reconstruct coastal wave height quite well after ~450–600 s.

In Figure 3e we observe similar features as in Figure 2e, where smoothing of the first few peaks occurs for both methods, but EnKF gets much closer to the true solution over time, and it is still able to capture the last peak at about 2,000 s very well. The accuracy of the coastal forecast is enhanced by assimilating more data, but much more so for EnKF than for OI. This contrast in forecast improvement can also be seen in Figure 3f, where the maximum wave height forecast for EnKF gets closer to the true solution and stays around that level for successive forecasts, but OI does not show any improvement after about 300 s. Rather, its forecast deteriorates, as the constant Kalman gain matrix can no longer accurately describe how interpolation should be performed between the model forecast and the data. EnKF also achieves a closer forecast of the arrival time of the maximum wave height and remains stable, whereas the OI forecast keeps fluctuating, especially after 600 s.

As most offshore networks suffer from large station spacing, EnKF offers a significant advantage in achieving more accurate and stable forecasts than OI.

6. Discussion and Conclusions

Our study demonstrates that EnKF achieves more accurate and stable forecasts compared to OI. The improvement in waveform agreement and coastal forecasts is most apparent when the station spacing is large. EnKF's outperformance can be attributed to the continual updating of the Kalman gain and covariance matrices, which minimizes the error variance of the forecast by better capturing the evolution of the physical process. However, the EnKF forecast accuracy depends on the choice of the initial error covariance matrix P_0, and we presently do not have a systematic way to select the error standard deviation for η and q. One idea is to run multiple tsunami scenarios in some region, with realistic sensor locations, and determine the error standard deviation that minimizes the misfit between the forecasts and the true solutions.

The increased accuracy and stability of EnKF relative to OI comes at the price of higher computational cost. This is especially true when utilizing Green's functions to forecast at certain points of interest along the coast (Wang et al., 2017). Nevertheless, EnKF can be easily parallelized by running each ensemble member on a separate processor, with further efficiency obtained by optimizing the wave propagation computation, for example, by using GPUs. With the advancement in high-performance computing and the potential availability of supercomputer queues dedicated to early warning, it is possible that EnKF can perform at speeds suitable for real-time implementation.

There are issues this study has not addressed that are essential to consider for future work on real-time tsunami early warning. First, the OBPG records include nonhydrostatic pressure changes due to seafloor deformation and seismic and ocean acoustic waves. We need to infer the ocean surface height from these records. A low-pass filter could remove the effects of seismic and ocean acoustic waves (Saito & Tsushima, 2016). The impact of seafloor deformation on the pressure record has been explored in the context of linear potential theory (Saito, 2013), and some studies propose using bias correction based on waveform inversion (Mulia et al., 2017) or assimilating using the time derivative of pressure (Tanioka, 2017). In addition, rather than rejecting seismic and ocean acoustic waves as noise, one could potentially use them to constrain tsunami or earthquake parameters (Kozdon & Dunham, 2014).

A second issue is accounting for dispersion in tsunami propagation that is not captured in the linear long-wave model. This will improve the quality of data assimilation for short wavelengths, as demonstrated by Wang et al. (2018), and EnKF can be extended in a straightforward manner to linear dispersive tsunami propagation equations.

Finally, recent studies have explored the use of multiple data sources in addition to OBPGs (Mulia et al., 2017; Wallace et al., 2016). For example, Global Navigation Satellite System receivers on commercial ships could constrain the initial tsunami wave height and be used directly to improve the EnKF forecast, while borehole observatory data and offshore seismic networks could improve the seismic inversion and indirectly constrain the initial seafloor displacement, which could be useful for denoising OBPG signals. The successful synthesis of various data sources will offer insight into the tsunami generation and propagation process in different subduction zones. The computational challenge remains, however, as we seek to integrate different models and data to produce real-time forecasts.

Acknowledgments
This work was supported by the National Science Foundation (EAR-1255439). We are grateful to Ossian O'Reilly for helping with the numerics. The source code is available at https://github.com/yyy910805/kalman-filter.

References

Aravkin, A. Y., Burke, J. V., & Pillonetto, G. (2014). Optimization viewpoint on Kalman smoothing with applications to robust and sparse estimation, *Compressed sensing & sparse filtering* (pp. 237–280). Verlag Berlin Heidelberg: Springer. https://doi.org/10.1007/978-3-642-38398-4_8

Blewitt, G., Hammond, W. C., Kreemer, C., Plag, H. P., Stein, S., & Okal, E. (2009). GPS for real-time earthquake source determination and tsunami warning systems. *Journal of Geodesy*, *83*, 335. https://doi.org/10.1007/s00190-008-0262-5

Evensen, G. (2003). The ensemble Kalman filter: Theoretical formulation and practical implementation. *Ocean Dynamics*, *53*(4), 343–367. https://doi.org/10.1007/s10236-003-0036-9

Gusman, A. R., Sheehan, A. F., Satake, K., Heidarzadeh, M., Mulia, I. E., & Maeda, T. (2016). Tsunami data assimilation of Cascadia seafloor pressure gauge records from the 2012 Haida Gwaii earthquake. *Geophysical Research Letters*, *43*, 4189–4196. https://doi.org/10.1002/2016GL068368

Hoshiba, M., & Ozaki, T. (2014). Earthquake early warning and tsunami warning of the Japan Meteorological Agency, and their performance in the 2011 off the Pacific coast of Tohoku earthquake (M_W 9.0), *Early warning for geological disasters* (pp. 1–28). Verlag Berlin Heidelberg: Springer. https://doi.org/10.1007/978-3-642-12233-0

Katzfuss, M., Stroud, J. R., & Wikle, C. K. (2016). Understanding the ensemble Kalman filter. *The American Statistician*, *70*(4), 350–357. https://doi.org/10.1080/00031305.2016.1141709

Kawaguchi, K., Kaneda, Y., & Araki, E. (2008). The z: A real-time seafloor research infrastructure for the precise earthquake and tsunami monitoring, *OCEANS 2008—MTS/IEEE Kobe Techno-Ocean* (pp. 1–4). Kobe, Japan: IEEE. https://doi.org/10.1109/ OCEANSKOBE.2008.4530918

Kozdon, J. E., & Dunham, E. M. (2014). Constraining shallow slip and tsunami excitation in megathrust ruptures using seismic and ocean acoustic waves recorded on ocean-bottom sensor networks. *Earth and Planetary Science Letters*, *396*, 56–65. https://doi.org/10.1016/j.epsl.2014.04.001

Kozdon, J. E., Dunham, E. M., & Nordström, J. (2013). Simulation of dynamic earthquake ruptures in complex geometries using high-order finite difference methods. *Journal of Scientific Computing*, *55*(1), 92–124. https://doi.org/10.1007/s10915-012-9624-5

Lotto, G. C., & Dunham, E. M. (2015). High-order finite difference modeling of tsunami generation in a compressible ocean from offshore earthquakes. *Computational Geosciences*, *19*(2), 327. https://doi.org/10.1007/s10596-015-9472-0

Lotto, G. C., Jeppson, T. N., & Dunham, E. M. (2018). Fully coupled simulations of megathrust earthquakes and tsunamis in the Japan Trench, Nankai Trough, and Cascadia Subduction Zone. *Pure and Applied Geophysics*, *175*, 1–33. https://doi.org/10.1007/s00024-018-1990-y

Ma, S. (2012). A self-consistent mechanism for slow dynamic deformation and tsunami generation for earthquakes in the shallow subduction zone. *Geophysical Research Letters*, *39*, L11310. https://doi.org/10.1029/2012GL051854

Madsen, H., & Canizares, R. (1999). Comparison of extended and ensemble Kalman filters for data assimilation in coastal area modelling. *International Journal for Numerical Methods in Fluids*, *31*(6), 961–981. https://doi.org/10.1002/(SICI)1097-0363(19991130)31:6<961::AID-FLD907>3.0.CO;2-0

Maeda, T., Obara, K., Shinohara, M., Kanazawa, T., & Uehira, K. (2015). Successive estimation of a tsunami wavefield without earthquake source data: A data assimilation approach toward real-time tsunami forecasting. *Geophysical Research Letters*, *42*, 7923–7932. https://doi.org/10.1002/2015GL065588

Melgar, D., Allen, R. M., Riquelme, S., Geng, J., Bravo, F., Baez, J. C., et al. (2016). Local tsunami warnings: Perspectives from recent large events. *Geophysical Research Letters*, *43*, 1109–1117. https://doi.org/10.1002/2015GL067100

Melgar, D., & Bock, Y. (2013). Near-field tsunami models with rapid earthquake source inversions from land-and ocean-based observations: The potential for forecast and warning. *Journal of Geophysical Research: Solid Earth*, *118*, 5939–5955. https://doi.org/10.1002/2013JB010506

Mulia, I. E., Inazu, D., Waseda, T., & Gusman, A. R. (2017). Preparing for the future Nankai Trough tsunami: A data assimilation and inversion analysis from various observational systems. *Journal of Geophysical Research: Oceans*, *122*, 7924–7937. https://doi.org/10.1002/2017JC012695

O'Reilly, O., Lundquist, T., Dunham, E. M., & Nordström, J. (2017). Energy stable and high-order-accurate finite difference methods on staggered grids. *Journal of Computational Physics*, *346*, 572–589. https://doi.org/10.1016/j.jcp.2017.06.030

Saito, T. (2013). Dynamic tsunami generation due to sea-bottom deformation: Analytical representation based on linear potential theory. *Earth, Planets and Space*, *65*(12), 1411–1423. https://doi.org/10.5047/eps.2013.07.004

Saito, T., & Tsushima, H. (2016). Synthesizing ocean bottom pressure records including seismic wave and tsunami contributions: Toward realistic tests of monitoring systems. *Journal of Geophysical Research: Solid Earth*, *121*, 8175–8195. https://doi.org/10.1002/2016JB013195

Tanioka, Y. (2017). Tsunami simulation method assimilating ocean bottom pressure data near a tsunami source region. *Pure and Applied Geophysics*, *175*, 721–729. https://doi.org/10.1007/s00024-017-1697-5

Thomson, R., Fine, I., Rabinovich, A., Mihály, S., Davis, E., Heesemann, M., & Krassovski, M. (2011). Observation of the 2009 samoa tsunami by the NEPTUNE-Canada cabled observatory: Test data for an operational regional tsunami forecast model. *Geophysical Research Letters*, *38*, L11701. https://doi.org/10.1029/2011GL046728

Titov, V. V., González, F. I., Bernard, E. N., Eble, M. C., Mofjeld, H. O., Newman, J. C., & Venturato, A. J. (2005). Real-time tsunami forecasting: Challenges and solutions, *Developing tsunami-resilient communities: The national tsunami hazard mitigation program* (pp. 184). Netherlands: Springer. https://doi.org/10.1007/1-4020-3607-8

Tonegawa, T., Araki, E., Kimura, T., Nakamura, T., Nakano, M., & Suzuki, K. (2017). Sporadic low-velocity volumes spatially correlate with shallow very low frequency earthquake clusters. *Nature Communications*, *8*(1), 2048. https://doi.org/10.1038/s41467-017-02276-8

Toomey, D. R., Allen, R. M., Barclay, A. H., Bell, S. W., Bromirski, P. D., Carlson, R. L., et al. (2014). The Cascadia initiative: A sea change in seismological studies of subduction zones. *Oceanography*, *27*(2), 138–150. https://doi.org/10.5670/oceanog.2014.49

Tsushima, H., Hino, R., Ohta, Y., Iinuma, T., & Miura, S. (2014). tFISH/RAPiD: Rapid improvement of near-field tsunami forecasting based on offshore tsunami data by incorporating onshore GNSS data. *Geophysical Research Letters*, *41*, 3390–3397. https://doi.org/10.1002/2014GL059863

Tsushima, H., Hirata, K., Hayashi, Y., Tanioka, Y., Kimura, K., Sakai, S., et al. (2011). Near-field tsunami forecasting using offshore tsunami data from the 2011 off the Pacific coast of Tohoku earthquake. *Earth, Planets and Space*, *63*(7), 56. https://doi.org/10.5047/eps.2011.06.052

Wallace, L. M., Araki, E., Saffer, D., Wang, X., Roesner, A., Kopf, A., et al. (2016). Near-field observations of an offshore M_w 6.0 earthquake from an integrated seafloor and subseafloor monitoring network at the Nankai Trough, southwest Japan. *Journal of Geophysical Research: Solid Earth*, *121*, 8338–8351. https://doi.org/10.1002/2016JB013417

Wang, Y., Satake, K., Maeda, T., & Gusman, A. R. (2017). Green's function-based tsunami data assimilation: A fast data assimilation approach toward tsunami early warning. *Geophysical Research Letters*, *44*, 10,282–10,289. https://doi.org/10.1002/2017GL075307

Wang, Y., Satake, K., Maeda, T., & Gusman, A. R. (2018). Data assimilation with dispersive tsunami model: A test for the Nankai Trough. *Earth, Planets and Space*, *70*(1), 131. https://doi.org/10.1186/s40623-018-0905-6

Xu, Z., & Song, Y. T. (2013). Combining the all-source Green's functions and the GPS-derived source functions for fast tsunami predictions—Illustrated by the March 2011 Japan tsunami. *Journal of Atmospheric and Oceanic Technology*, *30*(7), 1542–1554. https://doi.org/10.1175/JTECH-D-12-00201.1

Yamamoto, N., Hirata, K., Aoi, S., Suzuki, W., Nakamura, H., & Kunugi, T. (2016). Rapid estimation of tsunami source centroid location using a dense offshore observation network. *Geophysical Research Letters*, *43*, 4263–4269. https://doi.org/10.1002/2016GL068169